International Journal of Applied Electromagnetics and Mechanics 58 (2018) 239–260
DOI 10.3233/JAE-170034
IOS Press

Semianalytic integral method for the fast solution of circulating currents in power transformers

Guillermo A. Díaz Flórez[a,*], Enrique E. Mombello[b] and Geovanny A. Marulanda[c]
[a]*Electrical Engineering Department, Universidad de La Salle, 111711 Bogotá, Colombia*
[b]*Electrical Engineering Department, CONICET - Universidad Nacional de San Juan, J5400ARL San Juan, Argentina*
[c]*Electrical Engineering Department, Universidad de La Salle, 111711 Bogotá, Colombia*

Abstract. Power transformer design normally includes an optimization process which involves the assessment of a great number of design alternatives. This calculation process normally requires a high computation time and its reduction is always a desirable goal. Circulating currents in parallel connected conductors in transformer windings are a critical design aspect to be analyzed. This article presents a new methodology for the fast calculation of circulating currents for parallel connected conductors in power transformers. The formulation for solid conductor modeling has been developed using the same calculation strategy as in Semianalytic Integral Method (SAIM) [1], which allows a significant reduction of computational effort. A realistic case study of a 25 MVA transformer was used to validate the proposed methodology. As for the accuracy of the calculations, the comparison of the results obtained by the proposed methodology and those calculated using the Finite Element Method (FEM) shows an excellent agreement between both approaches. However, the computational performance of the new approach was found to be much higher than that of FEM. This makes the proposed method much more efficient for transformer design purposes.

Keywords: Circulating currents, power transformers, integral methods, skin depth

1. Introduction

Despite the great advances in the field of computing in the last decades, the optimization of power transformer design remains a challenging task, since account should be taken of dielectric, magnetic, thermal and constructive aspects [2].

One of the most important aspects of magnetic design is to keep eddy current losses in conductors within acceptable limits [3]. In order to achieve this, a widely used criterion is to ensure that the dimensions of the conductors do not significantly exceed the skin depth of the magnetic field δ[1].

*Corresponding author: Guillermo A. Díaz Flórez, Electrical Engineering Department, Universidad de La Salle, 111711 Bogotá, Colombia. Tel.: (571) 3535360; ext.: 2528-2529; E-mail: guandiaz@unisalle.edu.co.

[1]This criterion excludes foil conductor and solid bars with large cross sections, where the dimensions of the conductors can be considerably greater than δ

When transformers for large currents are required, there is no other way than to use parallel conductor arrangements in order to keep current density, ohmic losses and therefore temperature in suitable operational ranges.

Although the use of parallel conductor arrangements is an effective technique to keep the ohmic and eddy losses under control, there exist the disadvantage that each conductor belonging to a given turn is under the influence of different magnetic field values. This effect leads to the fact that induced voltages in the conductors of the same turn are not necessarily the same, giving rise to circulating currents between them [4].

In order to solve the problem of circulating currents, transpositions are made with the aim that all conductors are approximately linked by the same magnetic flux. Although the problem of circulating currents can be solved theoretically by making the complete transposition of the conductors, from a practical point of view, transpositions considerably increases the complexity, production times and consequently the costs of the coils.

Several studies can be found in the literature addressing the problem of the prediction of circulating currents and transposition optimization. Undoubtedly, the technique that offers the greatest precision for the calculation of circulating currents is a low-frequency magnetic field-electric circuit cosimulation using the finite element method (FEM) [5,6].

The calculation of circulating currents using FEM implies that the conductors must be discretized internally and an electric circuit must be used to define electrical connections between them. Because there are hundreds or even thousands of conductors and their dimensions are quite small compared to the overall dimensions of the active part, the simulation of this problem is quite demanding from a computational point of view, even using a 2D approach. Consequently, the calculation times of circulating currents using FEM are incompatible and even prohibitive for the design and optimization of transformers.

The methodology presented in this paper uses the same calculation strategy as in the Semianalytic Integral Method (SAIM), which was published in a previous work [1]. SAIM was used successfully to determine the current distribution in foil conductor windings considering eddy currents and the magnetic coupling with the magnetic core.

A new formulation of the magnetic coupling between conductors and the core is presented in this work. Additionally, circuit equations are introduced in order to model electrical connections between conductors.

A fast and precise methodology for the determination of the current distribution in a power transformer for an arbitrary electrical connection between conductors is proposed. In order to appreciate explicitly the effectiveness of the proposed method, an extreme case has been investigated where transpositions have not been used in the transformer winding.

2. Proposed model

This section introduces the concept of a low frequency equivalent magnetic model of the power transformer. In addition, the basic laws and principles used to formulate the methodology for the calculation of circulating currents are presented.

2.1. Transformer equivalent magnetic model

The power transformer has characteristics that make its modeling complex, such as its three-dimensionality and nonlinearities, so it is necessary to apply simplifications to the model so that the

solution is simpler, efficient and simultaneously a reasonable precision can be achieved [7]. A constant magnetic permeability of the core and a two-dimensional axisymmetric geometry are assumed in this work. The dimensions of the conductors and the electrical connections between them are modeled in detail.

The transformer modeling strategy used in this paper is based on replacing certain elements such as the iron core and conductors by magnetically equivalent arrangement of elements.

This novel modeling technique offers two advantages compared to numerical techniques such as FEM. On the one hand, there is a drastic reduction in the number of elements because only the boundary between the core and the air/oil is discretized. On the other hand, it is not necessary to discretize the conductors internally since the current inside them is modeled by a boundary condition related to the magnetic vector potential.

The core is replaced by an array of disc-shaped and cylinder-shaped elements, for which a boundary condition based on Ampere's law [1] is proposed. Figure 2 presents the arrangement of elements that make up the core. Note that because of space limitations, the detailed core model is not presented in this paper, since this subject is discussed in detail in [1]. This paper focuses mainly on modeling the conductors and their magnetic coupling to each other and to the core.

In order to be coherent throughout the article, the following definitions are proposed for the elements used to model the transformer:

- *Core*: Arrangement of cylindrical and disc-shaped surface elements having surface currents conceived as an equivalent of the high permeability ferromagnetic material.
- *Conductor*: Individual solid wire made of conductive material.
- *Turn*: Arrangement of one or more conductors electrically connected in parallel.
- *Coil*: Arrangement of one or more conductors electrically connected in series. This implies that the current flowing through all conductors belonging to a coil is the same.
- *Winding*: Arrangement of a certain amount of arbitrarily connected coils. In this article two windings are considered, the low voltage (LV) winding and the high voltage (HV) winding, both are made up of coils connected in parallel.

2.2. *Equivalent model of a conductor with rectangular cross-section*

Apart from the core, the other key element in the magnetic model of the transformer is the conductor. A schematic representation of a generic conductor is presented in Fig. 1(a), while Fig. 1(b) shows the equivalent circuit of a rectangular conductor, which has been represented by an impedance. Due to the resistive and inductive effects of the conductor, there is a voltage drop along it named $\underline{V}_{dp}$.

The equivalent magnetic model of a generic conductor is described by the following equation (see derivation in Appendix A.2).

$$\underline{V}_{dp} = -\underline{I}_{\phi} R_{DC} - \mathrm{j}\omega l_m \underline{A}_{\phi} \tag{1}$$

where $\underline{I}_{\phi}$ is the current through the conductor. R_{DC} is the DC resistance and l_m the mean length of the conductor. The magnetic vector potential at the center of the conductor is represented by $\underline{A}_{\phi}$. The angular frequency is $\omega = 2\pi f$ where f is the frequency of operation in Hz. Finally j is the imaginary unit.

Equation (1) is of crucial importance, since it relates the voltage drop, the current flowing in the conductor and the magnetic vector potential, where the latter models the inductive coupling with other conductors and the core. As will be seen, none of these three parameters $\underline{V}_{dp}$, $\underline{I}_{\phi}$ and $\underline{A}_{\phi}$ is usually known

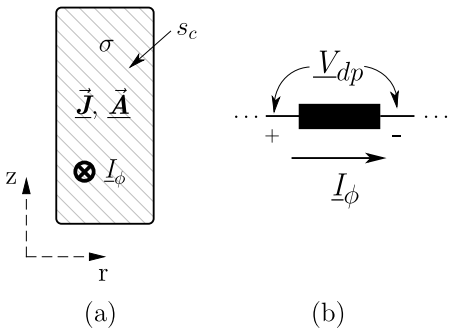

Fig. 1. (a) Geometric scheme of a solid rectangular conductor. (b) Equivalent circuit of a solid conductor.

in advance, however, it is possible to formulate a system of equations that allows the determination of these three variables for all transformer conductors.

3. Solution methodology

In this section, the model for the conductor of rectangular cross-section presented in Section 2.2 and the *core boundary equation* given in [1] are used to propose a mathematical model to determine both the current distribution of the core elements and the current in all conductors of the transformer.

3.1. Iron core equations

Figure 2 shows that the core has been represented using an amount of m_c surface elements, whose surface current densities ($\underline{K}_{\phi 1}^{[j]}$ and $\underline{K}_{\phi 2}^{[j]}$) are unknown.

In an earlier article the equivalent magnetic model of the core was presented in detail [1]. In [1] is shown that the following boundary condition is to be satisfied by the tangential component of the magnetic field strength at each field point of the core elements

$$\underline{H}_t^{[j]} = \frac{\kappa_m}{2}\nu^{[j]}\left(\underline{K}_{\phi 1}^{[j]} + \underline{K}_{\phi 2}^{[j]}\right) \tag{2}$$

where $\kappa_m = (1/2)(\mu_{r2}+1)(\mu_{r2}-1)$ and $\nu^{[j]}$ is defined as follows

$$\nu^{[j]} = \begin{cases} -1 & \text{for } j = 1 \cdots m_{yc}, \\ 1 & \text{for } m_{yc}+1 \cdots m_c, \end{cases} \tag{3}$$

where μ_{r2} is the relative magnetic permeability of the core material and m_{yc} is the number of elements used to model each yoke. It has been assumed that the number of elements used for the lower yoke and the upper yoke are the same.

The core is affected by the magnetic field produced by currents flowing in the low and high voltage windings which are composed of n_{LV} and n_{HV} conductors respectively. The currents in these windings are also unknown.

There are thus two different types of magnetic field sources. There are m_c surface field sources in the core, which are of the first type. The $n_{rc} = n_{LV} + n_{HV}$ cylindrical field sources with rectangular cross-section used to model the conductors of the low and high voltage windings belongs to the second type of sources. Accordingly, the transformer can be represented with a total amount of $n = m_c + n_{rc}$ elements.

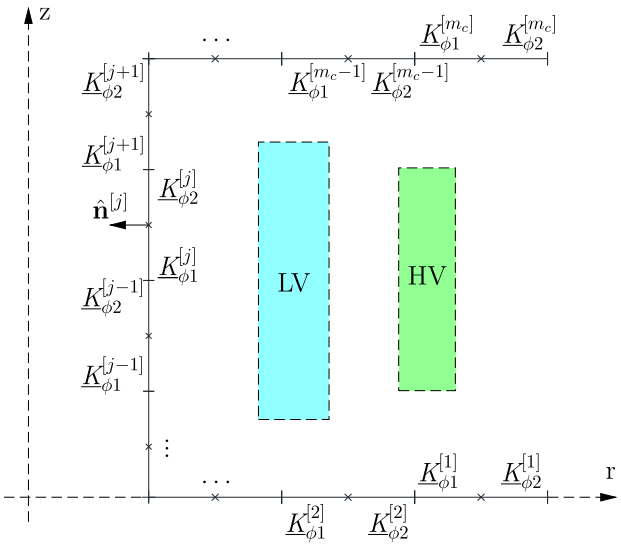

Fig. 2. General diagram of the transformer.

The tangential magnetic field component on the j-th core element produced by the i-th element can be written as

$$\underline{H}_t^{[j,i]} = k_{t1}^{[j,i]} \underline{K}_{\phi 1}^{[i]} + k_{t2}^{[j,i]} \underline{K}_{\phi 2}^{[i]} \quad \text{for } i = 1 \cdots m_c \text{ and } j = 1 \cdots m_c \tag{4}$$

where $k_{t1}^{[j,i]}$ and $k_{t2}^{[j,i]}$ are factors that depend exclusively on the dimensions and location of the element and the coordinate of the field point. Therefore, these factors are called *geometry-dependent factors*. On the other hand $\underline{K}_{\phi 1}^{[i]}$ and $\underline{K}_{\phi 2}^{[i]}$ are the surface current densities of the i-th element. The mathematical formulation to determine the geometry-dependent factors is available in [8] for the case of cylindrical surface elements and in [9] for the case of disc-shaped surface elements.

Equation (4) mathematically represents the mutual magnetic effect of the core elements. The contribution to the tangential component in the core due to the current flowing in the coil conductors can be written as follows

$$\underline{H}_t^{[j,i]} = k_t^{[j,i]} \underline{I}_{\phi}^{[i]} \quad \text{for } i = m_c + 1 \cdots n \text{ and } j = 1 \cdots m_c. \tag{5}$$

The mathematical expressions for determining the coefficients of the cylindrical elements with rectangular cross-section $k_t^{[j,i]}$ are given in Annex A.1. It should be noted that the magnetic field strength $\underline{H}_t^{[j,i]}$ can be associated either with the radial component or with the axial component according to the orientation of the core element on which the field is computed with respect to the overall coordinate system. In particular, the tangential field of the yoke is associated with the radial field component, while in the case of the core leg the tangential field is associated with the axial component of the field [1]. The tangential field strength in the j-th field point is the superposition of the effects of all elements and can be written as follows

$$\underline{H}_t^{[j]} = \sum_{i=1}^{n} \underline{H}_t^{[j,i]} \quad \text{for } j = 1 \cdots m_c. \tag{6}$$

Equation (6) can be rewritten for convenience as follows

$$\underline{H}_t^{[j]} = \underline{H}_t^{[j,j]} + \sum_{\substack{i=1 \\ i \neq j}}^{m_c} \underline{H}_t^{[j,i]} + \sum_{i=m_c+1}^{n} \underline{H}_t^{[j,i]}. \tag{7}$$

Substituting (4) and (5) into (7) gives

$$\underline{H}_t^{[j]} = k_{t1}^{[j,j]} \underline{K}_{\phi 1}^{[j]} + k_{t2}^{[j,j]} \underline{K}_{\phi 2}^{[j]} + \sum_{\substack{i=1 \\ i \neq j}}^{m_c} \left(k_{t1}^{[j,i]} \underline{K}_{\phi 1}^{[i]} + k_{t2}^{[j,i]} \underline{K}_{\phi 2}^{[i]} \right) + \sum_{i=m_c+1}^{n} \left(k_t^{[j,i]} \underline{I}_{\phi}^{[i]} \right) \quad \text{for } j = 1 \cdots m_c. \tag{8}$$

Substituting the core boundary condition (2) into (8) and rearranging gives the following expression

$$\left(\frac{\kappa_m}{2} \nu^{[j]} - k_{t1}^{[j,j]} \right) \underline{K}_{\phi 1}^{[j]} + \left(\frac{\kappa_m}{2} \nu^{[j]} - k_{t2}^{[j,j]} \right) \underline{K}_{\phi 2}^{[j]} - \sum_{\substack{i=1 \\ i \neq j}}^{m_c} \left(k_{t1}^{[j,i]} \underline{K}_{\phi 1}^{[i]} + k_{t2}^{[j,i]} \underline{K}_{\phi 2}^{[i]} \right) - \sum_{i=m_c+1}^{n} \left(k_t^{[j,i]} \underline{I}_{\phi}^{[i]} \right) = 0 \quad \text{for } j = 1 \cdots m_c. \tag{9}$$

Equation (9) represents a system of m_c equations with $2m_c + n_{rc}$ unknowns. The unknowns in this equation correspond to the current densities of the core elements $\underline{K}_{\phi 1}$, $\underline{K}_{\phi 2}$ ($2m_c$) and to the currents $\underline{I}_{\phi}$ (n_{rc}) in each of the conductors of the transformer. It should be noted that all coefficients $k_{t1}^{[j,j]}$, $k_{t2}^{[j,j]}$ and $k_t^{[j,i]}$ are known because they depend solely on transformer geometry.

3.2. Conductor equations

Figure 2 shows the general layout of the transformer. The LV and HV windings are schematically represented by a blue and a green box respectively. The conductor arrangement of the LV winding is shown in detail in Fig. 3. The arrangement of HV conductors is also shown in Fig. 4.

Note that the corresponding index is shown beside each conductor. It can also be seen that there is a blue x symbol at the geometric center of each element which denotes the field point where the magnetic vector potential will be calculated.

The inductive coupling between the core and each of the conductors is considered by means of the magnetic vector potential. Accordingly, the magnetic vector potential on the j -th element at an arbitrary conductor due to the i-th core element is given by

$$\underline{A}_{\phi}^{[j,i]} = k_{\phi 1}^{[j,i]} \underline{K}_{\phi 1}^{[i]} + k_{\phi 2}^{[j,i]} \underline{K}_{\phi 2}^{[i]} \quad \text{for } i = 1 \cdots m_c \text{ and } j = m_c + 1 \cdots n. \tag{10}$$

It should be noted that (10) represents the contribution of magnetic vector potential of each iron core element on every conductor. The contribution of the magnetic vector potential on a given conductor due

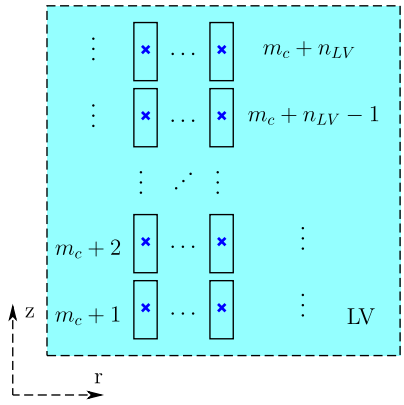

Fig. 3. Low voltage winding diagram.

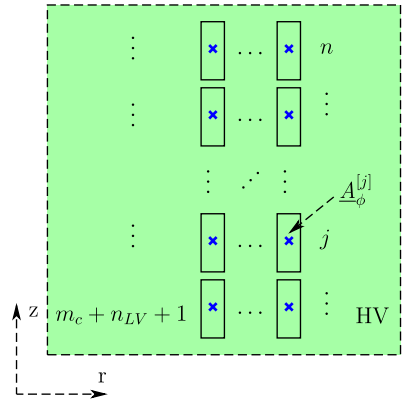

Fig. 4. High voltage winding diagram.

to other conductor including the conductor itself can be written as follows

$$\underline{A}_{\phi}^{[j,i]} = k_{\phi}^{[j,i]} \underline{I}_{\phi}^{[i]} \quad \text{for } i = m_c + 1 \cdots n \text{ and } j = m_c + 1 \cdots n. \tag{11}$$

Writing (1) for the case of the j-th element gives

$$\underline{V}_{dp}^{[j]} = -\underline{I}_{\phi}^{[j]} R_{DC}^{[j]} - \mathrm{j}\omega l_m^{[j]} \underline{A}_{\phi}^{[j]} \tag{12}$$

where $\underline{A}_{\phi}^{[j]}$ is the total magnetic vector potential present at the field point of the j-th element as a consequence of the contribution of all elements including the given element itself.

$$\underline{A}_{\phi}^{[j]} = \sum_{i=1}^{m_c} \underline{A}_{\phi}^{[j,i]} + \sum_{i=m_c+1}^{n} \underline{A}_{\phi}^{[j,i]}. \tag{13}$$

Substituting (10), (11) and (13) into (12) and after performing some algebraic manipulations yields

$$\begin{aligned} &\mathrm{j}\omega l_m^{[j]} \sum_{i=1}^{m_c} \left(k_{\phi 1}^{[j,i]} \underline{K}_{\phi 1}^{[i]} + k_{\phi 2}^{[j,i]} \underline{K}_{\phi 2}^{[i]} \right) + \underline{I}_{\phi}^{[j]} \left(R_{DC}^{[j]} + \mathrm{j}\omega l_m^{[j]} k_{\phi}^{[j,j]} \right) \\ &+ \mathrm{j}\omega l_m^{[j]} \sum_{\substack{i = m_c + 1 \\ i \neq j}}^{n} \left(k_{\phi}^{[j,i]} \underline{I}_{\phi}^{[i]} \right) + \underline{V}_{dp}^{[j]} = 0 \quad \text{for } j = m_c + 1 \cdots n. \end{aligned} \tag{14}$$

Note that (14) represents a system of n_{rc} equations, however n_{rc} unknowns associated with the voltage drop $\underline{V}_{dp}^{[j]}$ of each conductor have also been added to the equation system. According to the above, (9) and (14) represent a system of n equations with $2m_c + 2n_{rc}$ unknowns, so $m_c + n_{rc}$ equations are needed to obtain a complete system.

3.3. Equations linking surface elements

A conclusion drawn in the previous section was that additional equations related to the core are required. As seen in Fig. 2, the surface current density at the end of an element coincides with the current density of the next element. Taking advantage of this situation, the following set of equations can be posed

$$\begin{aligned} &\underline{K}_{\phi 1}^{[j]} - \underline{K}_{\phi 2}^{[j+1]} = 0 \quad \text{for } j = 1 \cdots m_{yc} - 1 \\ &\underline{K}_{\phi 1}^{[j]} - \underline{K}_{\phi 1}^{[j+1]} = 0 \quad \text{for } j = m_{yc} \\ &\underline{K}_{\phi 2}^{[j]} - \underline{K}_{\phi 1}^{[j+1]} = 0 \quad \text{for } j = m_{yc} + 1 \cdots m_c - 1 \\ &\underline{K}_{\phi 2}^{[1]} - \underline{K}_{\phi 2}^{[m_c]} = 0. \end{aligned} \tag{15}$$

Equation set (15), not only provides m_c additional equations, but also allows the surface current density to be distributed smoothly and continuously along the yokes and the core leg.

3.4. Circuit equations for conductor elements

In addition to the relationships between core surface elements it is also necessary to model the circuit connections between conductors of each winding.

Because these electrical connections are specific for each transformer, and in order to make a clear presentation of this subject, the corresponding equations are presented in Section 4.2.2 for the particular case study of a 25 MVA transformer.

4. Implementation of the proposed methodology

4.1. Case study description

Table 1 shows general information of the transformer core. Table 2 and Table 3 give geometric information of the high and low voltage windings respectively.

Table 1
General parameters of the transformer

Parameter	Value
General information	
Rated power	25 MVA
Connection group	Dyn1
Nominal frequency	50 Hz
Nominal primary voltage	69 000 Vrms
Taps (OLTC)	$+/-8 \times 1.25\%$
Rated secondary voltage	24 000 Vrms
Iron core	
Core type	Stacked-Laminated
Window height	1086 mm
Window width	658 mm
Leg diameter	544 mm
Relative magnetic permeability	10 000

Table 2
Construction data of the case study LV winding

Parameter	Value
Winding type	Layers
Conductor material	Copper
Bare conductor radial dimension	3.4 mm
Bare conductor axial dimension	13.6 mm
Inner winding radius	285 mm
Winding radial dimension	94.9 mm
Winding axial dimension	923.6 mm
Distance to the lower yoke	76 mm
Number of layers	16
Number of turns per layer	11
Number of turns	176
Number of parallel axial conductors	6

The case study is a three-phase 25 MVA - 69 kV transformer. The LV winding is the innermost winding, layer-type, star connected. A single turn of the LV winding consist of 6 axial parallel conductors. On the other hand, the HV winding is the outermost one, disk-type, delta connected. A single turn of the HV winding consist of 3 radial parallel conductors. Figure 9 shows the uppermost part of the core window with the physical layout of the conductors. For the sake of simplicity, it has been assumed that the conductor arrangement is uniform along the winding cross-section.

It is also important to note that this transformer has an on-load tap-changer (OLTC) connected to a third independent winding. Because the simulation is done for the rated tap and the turn distribution of the tap winding is symmetrical, this winding is not connected in this condition and was not included in the simulations.

The actual transformer design considers a transposition at the central part of the high voltage winding so that the average lengths of the three conductors forming a turn are approximately the same. Since the

Table 3
Construction data of the case study HV winding

Parameter	Value
Winding type	Disks
Conductor material	Copper
Bare conductor radial dimension	2.4 mm
Bare conductor axial dimension	9 mm
Inner winding radius	405 mm
Winding radial dimension	130.9 mm
Winding axial dimension	952.9 mm
Distance to the lower yoke	61 mm
Number of disks	73
Number of turns per disc	12
Number of turns	876
Number of parallel radial conductors	3

purpose of this work is to evaluate the performance of a new calculation method for the case of circulating currents between conductors connected in parallel, the radial transposition has been intentionally ignored to intensify the effect of circulating currents and to be able to appreciate the phenomenon more explicitly.

Despite the fact that the transpositions have been ignored in the case study, it will be seen that the proposed methodology is flexible enough to consider arbitrary circuit connections between conductors. This makes it possible to model transpositions, turns which are switched off by the tap changer, or faults due to short-circuits between conductors.

4.2. Simulation using SAIM

This section provides an overview of the most important considerations for the modeling of the case study transformer using SAIM. The modeling of the core is performed using the equivalent magnetic model presented in Fig. 2. A total amount of $m_c = 101$ elements has been used for the core, of which $m_{yc} = 23$ belong to the lower and upper yokes.

In the case of winding conductors, $n_{LV} = 1056$ solid cylindrical elements have been used for the LV winding and $n_{HV} = 2628$ elements for the HV winding. The total number of solid cylindrical elements is $n_{rc} = n_{LV} + n_{HV} = 3684$. Each of these solid cylindrical elements represents the magnetic effect of the corresponding transformer conductor. The total number of elements (laminar + solid) used in the model is $n = m_c + n_{rc} = 3785$.

As a starting point, SAIM requires the exact location of all core and conductor elements as input data. This information is used to determine all *geometry-dependent factors*. Further information is also required on the circuit connections between conductors and on at least one current or voltage source.

4.2.1. Conductor identification and electrical connections

The rules used to assign indices to the conductor elements of the windings are presented in this section. Figure 5(a) shows a sketch of the low voltage winding. As can be seen, the identification number (ID) of the innermost and lowermost conductor of the winding is 102. This is because each element has a unique number, and since the core has 101 elements, the index of the first conductor is the next integer.

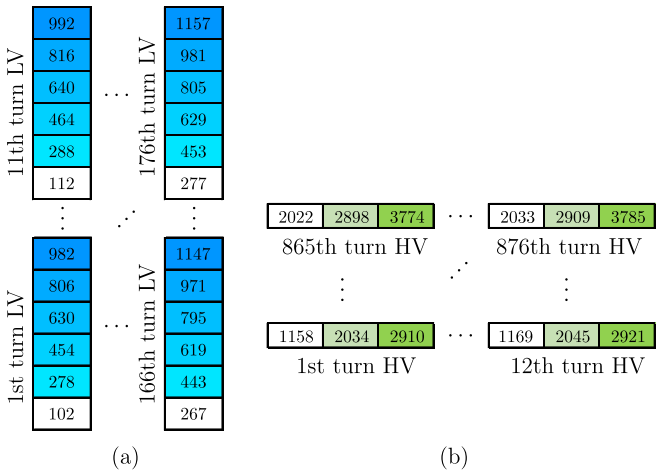

Fig. 5. (a) Identification of LV winding conductors. (b) Identification of HV winding conductors.

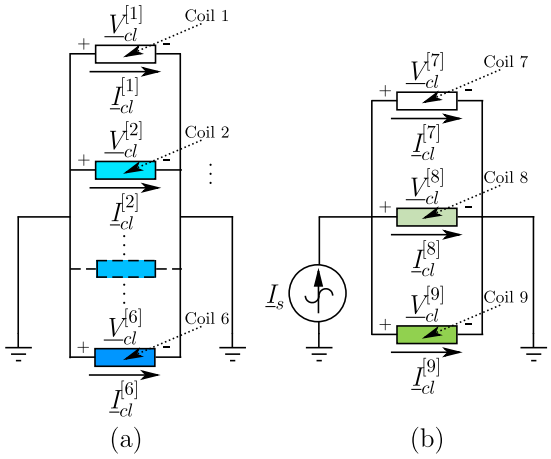

Fig. 6. (a) Coil connections for the LV winding. (b) Coil connections for the HV winding.

Because the LV winding is a layer winding and each turn has 6 axial conductors connected in parallel, the conductor with the next index is the conductor which is in series with the element number 102, which corresponds to the lowest conductor of the second turn. Note that in Fig. 5 the lowest conductors of each turn have a white background. Since the LV winding has 176 turns, the index of the lowest conductor of the last turn is 277.

The conductors connected in series have been represented using the same background color in Fig. 5, and using a gradated color scale from white to dark blue. Note that the index of the uppermost LV conductor of the last turn (176) is indexed 1157, which is consistent considering that the sum of the total number of conductors and the total number of core elements is $101 + 176 \times 6 = 1157$.

Just as for the LV winding, Fig. 5(b) shows the ID of the HV winding elements. As can be seen, the next ID number corresponds to the innermost and lowermost conductor of the HV winding, whose index is 1158. The conductors connected in series have been represented using the same background color, this

time using a gradated color scale from white to dark green. The ID of the last HV conductor is 3785 which is equal to n, as expected.

Figure 6(a) shows a circuit representing the electrical connections of the coils of the LV winding.

The LV winding has 6 coils connected in parallel and connected on both sides to the reference potential. This connection represents the short circuit test, where the terminals of the LV winding are short-circuited.

On the other hand, Fig. 5(b) depicts the connections of the coils of the HV winding. There are three parallel coils connected to a current source $\underline{I}_s$. In this case, the current feeding the circuit is the rated single-phase peak current of the HV winding, that is, $\underline{I}_s = \sqrt{2} \cdot 120.8$ A. This value is the current to be used in the transformer short-circuit test. It should be noted from Fig. 6 that the current flowing in the coils is $\underline{I}_{cl}^{[c]}$, whereas the electric potential for each of them is denoted $\underline{V}_{cl}^{[c]}$ where c =1⋯9. Note that each coil is composed of a arrangement of series connected conductors, which is described in detail in the next section.

4.2.2. Equations of electrical connections between conductors

The m_c additional equations related to the core have been given in Section 3.3. However, n_{rc} additional equations are still required to obtain a complete system. In this section, the missing equations representing the electrical connections between conductors will be presented.

Figure 7 depicts the detailed electrical connection between conductors of the LV coils is schematically shown. The color has been consistently chosen according to the definition of the coils and the identification of the conductors.

A set of n_{LV} =1056 additional equations linking the current in the conductors to the currents in the LV coils is given in (16).

$$\begin{aligned}
&\underline{I}_{\phi}^{[102]} = \underline{I}_{cl}^{[1]}, \underline{I}_{\phi}^{[103]} = \underline{I}_{cl}^{[1]}, \dots, \underline{I}_{\phi}^{[277]} = \underline{I}_{cl}^{[1]} \\
&\underline{I}_{\phi}^{[278]} = \underline{I}_{cl}^{[2]}, \underline{I}_{\phi}^{[279]} = \underline{I}_{cl}^{[2]}, \dots, \underline{I}_{\phi}^{[453]} = \underline{I}_{cl}^{[2]} \\
&\underline{I}_{\phi}^{[454]} = \underline{I}_{cl}^{[3]}, \underline{I}_{\phi}^{[455]} = \underline{I}_{cl}^{[3]}, \dots, \underline{I}_{\phi}^{[629]} = \underline{I}_{cl}^{[3]} \\
&\underline{I}_{\phi}^{[630]} = \underline{I}_{cl}^{[4]}, \underline{I}_{\phi}^{[631]} = \underline{I}_{cl}^{[4]}, \dots, \underline{I}_{\phi}^{[805]} = \underline{I}_{cl}^{[4]} \\
&\underline{I}_{\phi}^{[806]} = \underline{I}_{cl}^{[5]}, \underline{I}_{\phi}^{[807]} = \underline{I}_{cl}^{[5]}, \dots, \underline{I}_{\phi}^{[981]} = \underline{I}_{cl}^{[5]} \\
&\underline{I}_{\phi}^{[982]} = \underline{I}_{cl}^{[6]}, \underline{I}_{\phi}^{[983]} = \underline{I}_{cl}^{[6]}, \dots, \underline{I}_{\phi}^{[1157]} = \underline{I}_{cl}^{[6]}.
\end{aligned} \tag{16}$$

Similarly, Fig. 8 shows the electrical connections between HV conductors, whereas the corresponding set of equations is presented in (17), which provides n_{HV} = 2628 additional equations.

$$\begin{aligned}
&\underline{I}_{\phi}^{[1158]} = \underline{I}_{cl}^{[7]}, \underline{I}_{\phi}^{[1159]} = \underline{I}_{cl}^{[7]}, \dots, \underline{I}_{\phi}^{[2033]} = \underline{I}_{cl}^{[7]} \\
&\underline{I}_{\phi}^{[2034]} = \underline{I}_{cl}^{[8]}, \underline{I}_{\phi}^{[2035]} = \underline{I}_{cl}^{[8]}, \dots, \underline{I}_{\phi}^{[2909]} = \underline{I}_{cl}^{[8]} \\
&\underline{I}_{\phi}^{[2910]} = \underline{I}_{cl}^{[9]}, \underline{I}_{\phi}^{[2911]} = \underline{I}_{cl}^{[9]}, \dots, \underline{I}_{\phi}^{[3785]} = \underline{I}_{cl}^{[9]}.
\end{aligned} \tag{17}$$

It should be noted that (16) and (17) provide an amount of $n_{LV} + n_{HV}$ additional equations. However, 9 additional unknowns $\underline{I}_{cl}^{[c]}$ (with c =1⋯9) related to the coil currents have been added to the problem.

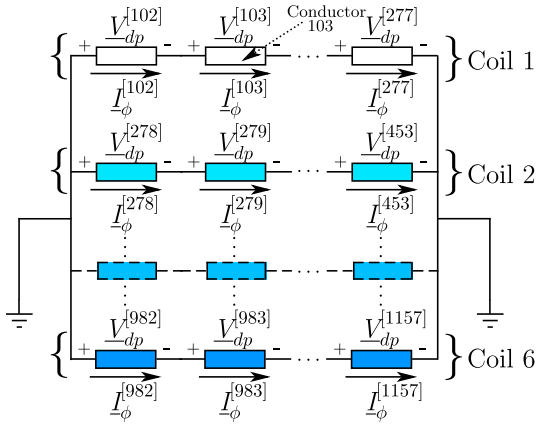

Fig. 7. Electrical connections between LV elements.

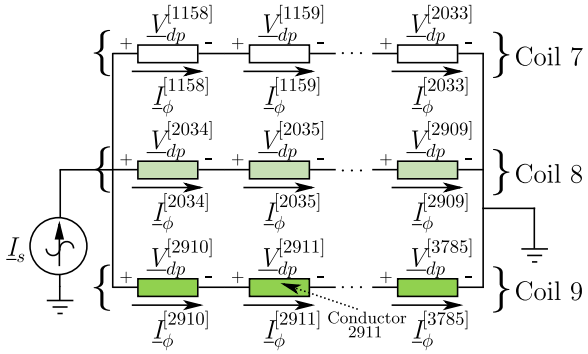

Fig. 8. Electrical connections between HV elements.

In order to obtain a complete system, it is necessary to propose additional equations. It can be seen from Fig. 6(b) that the sum of the currents of the three coils must be equal to the current of the source $\underline{I}_s$, so that

$$\underline{I}_{cl}^{[7]} + \underline{I}_{cl}^{[8]} + \underline{I}_{cl}^{[9]} = \underline{I}_s. \tag{18}$$

On the other hand, the equations of the coil voltages of the LV winding can be presented as follows

$$\begin{aligned}
&\underline{V}_{dp}^{[102]} + \underline{V}_{dp}^{[103]} + \cdots + \underline{V}_{dp}^{[277]} = \underline{V}_{cl}^{[1]} \\
&\underline{V}_{dp}^{[278]} + \underline{V}_{dp}^{[279]} + \cdots + \underline{V}_{dp}^{[453]} = \underline{V}_{cl}^{[2]} \\
&\underline{V}_{dp}^{[454]} + \underline{V}_{dp}^{[455]} + \cdots + \underline{V}_{dp}^{[629]} = \underline{V}_{cl}^{[3]} \\
&\underline{V}_{dp}^{[630]} + \underline{V}_{dp}^{[631]} + \cdots + \underline{V}_{dp}^{[805]} = \underline{V}_{cl}^{[4]} \\
&\underline{V}_{dp}^{[806]} + \underline{V}_{dp}^{[807]} + \cdots + \underline{V}_{dp}^{[981]} = \underline{V}_{cl}^{[5]} \\
&\underline{V}_{dp}^{[982]} + \underline{V}_{dp}^{[983]} + \cdots + \underline{V}_{dp}^{[1157]} = \underline{V}_{cl}^{[6]}.
\end{aligned} \tag{19}$$

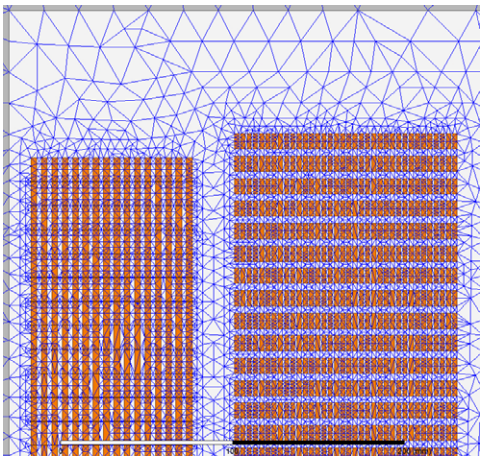

Fig. 9. Final mesh at the upper part of the core window (Ansys Maxwell).

Similarly, the expressions for the voltages of the coils of the HV winding can be set up as follows

$$\begin{aligned}
&\underline{V}_{dp}^{[1158]} + \underline{V}_{dp}^{[1159]} + \cdots + \underline{V}_{dp}^{[2033]} = \underline{V}_{cl}^{[7]} \\
&\underline{V}_{dp}^{[2034]} + \underline{V}_{dp}^{[2035]} + \cdots + \underline{V}_{dp}^{[2909]} = \underline{V}_{cl}^{[8]} \\
&\underline{V}_{dp}^{[2910]} + \underline{V}_{dp}^{[2911]} + \cdots + \underline{V}_{dp}^{[3785]} = \underline{V}_{cl}^{[9]}.
\end{aligned} \tag{20}$$

The following expressions model the parallel connection of the LV coils and the connection to the reference voltage.

$$\begin{aligned}
&\underline{V}_{cl}^{[1]} = 0, \underline{V}_{cl}^{[2]} = \underline{V}_{cl}^{[1]}, \underline{V}_{cl}^{[3]} = \underline{V}_{cl}^{[2]} \\
&\underline{V}_{cl}^{[4]} = \underline{V}_{cl}^{[3]}, \underline{V}_{cl}^{[5]} = \underline{V}_{cl}^{[4]}, \underline{V}_{cl}^{[6]} = \underline{V}_{cl}^{[5]}.
\end{aligned} \tag{21}$$

Finally, the equation for the parallel connection of the HV winding coils is

$$\underline{V}_{cl}^{[8]} = \underline{V}_{cl}^{[7]}, \underline{V}_{cl}^{[9]} = \underline{V}_{cl}^{[8]}. \tag{22}$$

In summary, the final set of equations to be solved consists of the following set of equations: (9), (14), (15), and (16) to (22). These equations represent a system with a total amount of 7588 equations with 7588 unknowns. Table 4 summarizes the equations that compose the final system to be solved numerically. This table also shows the number of unknowns and equations added to the system so that a complete system is finally obtained.

It is relatively simple to set up a system of equations in matrix form as $\underline{\mathbf{M}} \cdot \underline{\mathbf{x}} = \underline{\mathbf{b}}$ which can be efficiently solved using Matlab or Octave. The solution has been computed using Matlab, and no conditioning problems have been found, so the system can be solved reliably by the LU factorization method. The equivalent current distribution in the core, the currents and voltage drops in the conductors and the currents and voltages of the coils can be obtained directly from the solution of the equation system.

Table 4
Summary of the equations solved using SAIM

Equation number	Added equations	Added unknowns	Description
(9)	101 (m_c)	3886 ($2m_c + n_{rc}$) $\underline{K}_{\phi 1}$,$\underline{K}_{\phi 2}$, $\underline{I}_{\phi}$	Magnetic effects on all core elements.
(14)	3684 (n_{rc})	3684 (n_{rc}) $\underline{V}_{dp}$	Magnetic effects of all elements on the conductors.
(15)	101 (m_c)	0 -	Linking equations between core elements.
(16)	1056 (n_{LV})	6 $\underline{I}_{cl}$	Relationships between conductor currents of LV coils.
(17)	2628 (n_{HV})	3 $\underline{I}_{cl}$	Relationships between conductor currents of HV coils.
(18)	1	0 -	Current source at HV coils.
(19)	6	6 $\underline{V}_{cl}$	Relationships between conductor voltages of LV coils.
(20)	3	3 $\underline{V}_{cl}$	Relationships between conductor voltages of HV coils.
(21)	6	0 -	Parallel connections of LV coils.
(22)	2	0 -	Parallel connections of HV coils.
	7588	7588	Total amount of equations and unknowns.

4.3. Simulation using FEM

The case study was modeled in detail using FEM by means of Ansys Maxwell 17.1.0 software on a PC Core i7 2.8 GHz, 16 GB RAM. A 2D axisymmetric model has been used representing the core and the LV and HV conductors. Using a Python script, the *Net List* file containing information about the electrical connections of the transformer conductors was created. The Magnetic Eddy Current low-frequency harmonic solver has been used for the simulation of the case study.

Figure 9 shows the final mesh generated by Ansys Maxwell. Note that because the conductors are modeled as solid elements, the program generates mesh inside the conductors to be able to determine the solution of the current distribution, which appreciably affects the performance of the solution using FEM.

4.4. Comparison of results given by FEM and SAIM

Table 5 presents a general summary of FEM simulations. Note that it is easy to calculate power losses in the conductors because the solution of the current distribution of both the core and the conductors

Table 5
Summary of simulations using FEM and SAIM

Parameter	FEM	SAIM
Single-phase total losses LV + HV (kW)	58.18	58.61
Short-circuit voltage (kVrms)	9.13	8.93
Total number of elements	76 841	3 785
Total number of degrees of freedom	314 776	7 588
Total time	9 min, 42 s	37.2 s

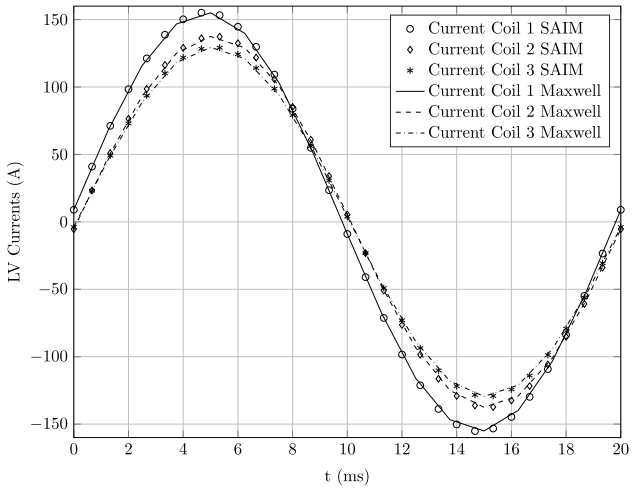

Fig. 10. Currents in the LV coils 1, 2 and 3.

is known [3]. On the other hand, the calculated coil voltages $\underline{V}_{cl}^{[7]} \cdots \underline{V}_{cl}^{[9]}$ directly gives the short circuit voltage of the short circuit test, which is also given in Table 5.

It is important to highlight that the total simulation time using FEM is close to 10 minutes, and the total simulation time using the proposed methodology is 37.2 seconds. This last computation time is quite adequate for transformer design purposes considering the complexity of the case study, which is composed of an arrangement of 3 684 conductors each interconnected in a circuit network. The time taken to create the geometry, to establish the sources and boundary conditions, and to calculate the solution has been considered in both cases.

It can be seen from Figs 10 and 11 that the currents of the coils of the LV winding are not the same. Differences close to 30 A are observed in the peak values of currents. This indicates the existence of circulating currents in the LV conductors. It is interesting to note that the existence of these circulating currents in LV is not explained by the different resistance of the conductors, since in the case of a layer winding all conductors have exactly the same length.

The only explanation for these currents is a difference in the average flux linkage of the conductors, which is a consequence of the asymmetry of the windings with respect to the core window.

Furthermore, Fig. 12 shows the current distribution of the HV winding coils. There are marked differences not only in the amplitudes but also in the phase angles of the currents. Finally, it is important to point out that the solution of the currents of the LV winding coils are totally coherent with the physical

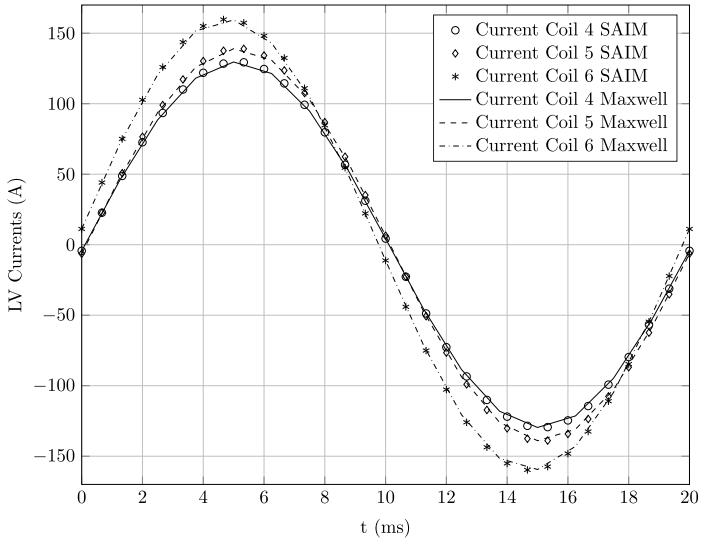

Fig. 11. Currents of the LV coils 4, 5 and 6.

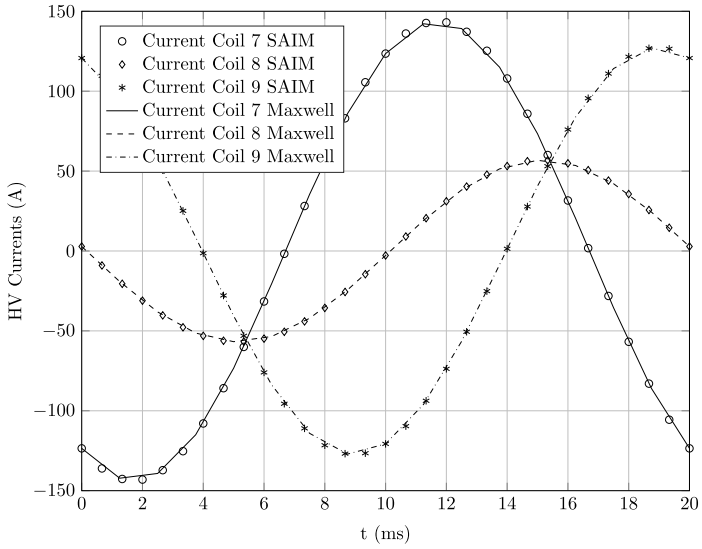

Fig. 12. Currents of the HV coils 7, 8 and 9.

behavior of a transformer, that is, when adding the currents $\underline{I}_{cl}^{[1]} + \cdots + \underline{I}_{cl}^{[6]}$ the rated phase current of the LV winding is obtained. The interesting fact is that this value arises from the simulation and has not been explicitly specified as input data of the problem.

5. Conclusion

This work presents a novel method to determine the distribution of circulating currents in transformers windings. Whereas the accuracy of the proposed approach is comparable to that of FEM, the computational effort by using the first method is considerably lower. This is a remarkable advantage for applications like the optimization stage of transformer design process.

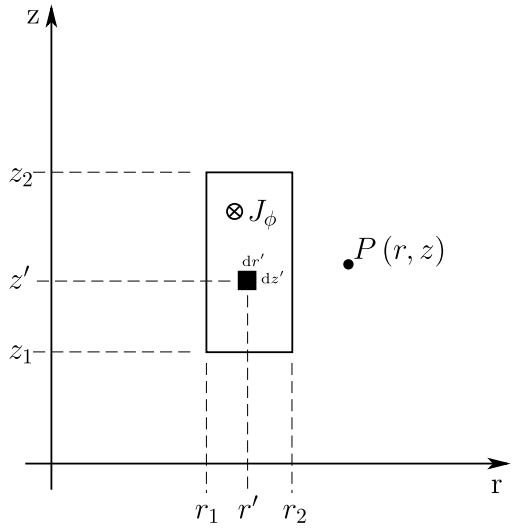

Fig. 13. Cylinder with rectangular cross-section.

The proposed method is based on equivalent magnetic models of both the core and the conductors, which do not involve a discretization of the inner part of them. This leads to a considerably reduction of the size of the problem compared to traditional techniques such as FEM. An important stage of the development was to set up equations for the different components of the model and also equations to link them each other.

The approach presented has been successfully validated using a case study of a power transformer having two windings (LV and HV); nevertheless, it can be applied to an arbitrary number of windings, and arbitrary connections can be established between them. This is very useful for the analysis of extreme cases such as the detailed modeling of connections between a tap winding and the main winding of transformers having an OLTC, or as in the case autotransformers.

Appendix

A.1. Geometry-dependent factors for a cylinder with rectangular cross-section

The purpose of this section is to present the equations for determining geometry-dependent factors of a cylinder with rectangular cross-section of arbitrary dimensions for an arbitrary evaluation point. Consider a general cylinder like the one shown in Fig. 13.

The magnetic field produced by the cylinder at certain field point can be written as the product of the current $\underline{I}_\phi$ by a factor that depends only on the cylinder geometry and the coordinates of the field point (k_ϕ, k_r and k_z). According to the above, the magnetic vector potential and the radial and axial components of the magnetic field strength can be written as follows

$$\underline{A}_\phi = k_\phi \underline{I}_\phi, \underline{H}_r = k_r \underline{I}_\phi, \underline{H}_z = k_z \underline{I}_\phi. \tag{A.1}$$

The geometry-dependent factors can be written as follows

$$k_\phi = \frac{\mu_0}{2\pi s_c}\int_0^\pi \left(\zeta_1\Big|_{z'=z_1}^{z'=z_2}\Big|_{r'=r_1}^{r'=r_2}\right)\mathrm{d}\phi' \tag{A.2}$$

$$k_r = -\frac{1}{2\pi s_c}\int_0^\pi \left(\zeta_2\Big|_{z'=z_1}^{z'=z_2}\Big|_{r'=r_1}^{r'=r_2}\right)\mathrm{d}\phi' \tag{A.3}$$

$$k_z = \frac{1}{2\pi s_c}\int_0^\pi \left(\zeta_3\Big|_{z'=z_1}^{z'=z_2}\Big|_{r'=r_1}^{r'=r_2}\right)\mathrm{d}\phi' \tag{A.4}$$

where s_c is the cross-sectional of the cylinder.

$$\zeta_1 = \frac{1}{2}\cos(\phi')\xi_2$$
$$\zeta_2 = -\xi_1\cos(\phi') - r\cos(\phi')^2\log(r' + \xi_1 - r\cos(\phi'))$$
$$\zeta_3 = (z - z')\xi_3$$

$$\begin{aligned}
\xi_1 &= \sqrt{r^2 + r'^2 + (z-z')^2 - 2rr'\cos(\phi')}\\
\xi_2 &= -\xi_1 z + \xi_1 z' + \left(r^2\cos(2\phi') - r'^2\right)\log(\xi_1 + z - z')\\
&\quad + 2r\cos(\phi')\left((z'-z)\log(r' + \xi_1 - r\cos\phi') - z'\right)\\
&\quad - r^2\sin(2\phi')\tan^{-1}\left(\frac{(z-z')(r\cos(\phi') - r')\csc(\phi')}{r\xi_1}\right) + r^2\sin(2\phi')\tan^{-1}\left(\frac{r\sin(\phi')}{z-z'}\right)\\
\xi_3 &= -\log(r' + \xi_1 - r\cos(\phi')) + r\sin(\phi')\left[\frac{\tan^{-1}\left(\frac{|z-z'|(r'-r\cos(\phi'))\csc(\phi')}{r\xi_1}\right)}{|z-z'|}\right]\\
&\quad + r\sin(\phi')\left[\frac{rr'\sin(\phi')}{\xi_1\left(r^2 + r'^2 - 2rr'\cos(\phi')\right)}\right].
\end{aligned}$$

Although references [10] and [11] present the mathematical expressions for the magnetic field produced by a current carrying conductor with rectangular cross section, the expressions presented above are more convenient due to their simplicity and to the fact that the geometry-dependent component has been factorized.

A.2. Derivation of the boundary equation for the conductor with rectangular cross-section

Assume a solid conductor with a rectangular cross-section through which a sinusoidal current $\underline{I_\phi}$[2] flows in the direction of the azimuth angle $\hat{\boldsymbol{\phi}}$. The conductor has conductivity σ and a cross-section s_c. The conductor is assumed to be located parallel to the x-y plane, and that its axis coincides with the z-axis. A cross-section of the conductor is shown in Fig. 1(a).

The magnetic vector potential $\underline{\vec{A}}$ in the conductor is a consequence of the superposition of the magnetic effects of the currents flowing in all conductors, including the given conductor, and the magnetizing currents in the core.

[2]The line below the variable name indicates its sinusoidal nature denoted as a phasor.

It is assumed in this paper that all currents are sinusoidal with frequency ω. Since this is a sinusoidal steady state problem, the current density $\underline{\vec{J}}$ in the conductor of Fig. 1(a) can be represented as the superposition of the eddy current component $\underline{\vec{J}}_{eddy}$ and the source voltage component $\underline{\vec{J}}_{src}$ as follows

$$\underline{\vec{J}} = \underline{\vec{J}}_{eddy} + \underline{\vec{J}}_{src}. \tag{A.5}$$

Similarly, the current can be decomposed into two components as follows [12]

$$\underline{I}_{\phi} = \underline{I}_{eddy} + \underline{I}_{src}. \tag{A.6}$$

The magnetic vector potential is related to the eddy current density as follows

$$\underline{\vec{J}}_{eddy} = -\mathrm{j}\sigma\omega\underline{\vec{A}} \tag{A.7}$$

where the magnetic vector potential $\underline{\vec{A}}$ in the given conductor corresponds to the total field produced by all conductors (including the conductor itself) and the iron core. Furthermore, the source current density associated with the electric potential is given by

$$\underline{\vec{J}}_{src} = -\sigma\nabla\underline{V} \tag{A.8}$$

where $\underline{V}$ is a scalar field representing the electric potential distribution along the conductor. On the other hand, the eddy current can be calculated by means of the following surface integral

$$\underline{I}_{eddy} = \int_{S'} \underline{\vec{J}}_{eddy} \cdot \mathrm{d}\vec{\mathbf{s}}. \tag{A.9}$$

Substitution of (A.7) into (A.9) yields

$$\underline{I}_{eddy} = -\mathrm{j}\sigma\omega \int_{S'} \underline{\vec{A}} \cdot \mathrm{d}\vec{\mathbf{s}}. \tag{A.10}$$

As the problem axisymmetric, the equation $\underline{\vec{A}} = \underline{A}_{\phi}\hat{\boldsymbol{\phi}}$ holds, where $\hat{\boldsymbol{\phi}}$ is the azimuthal unit vector. On the other hand, the differential of surface is $\mathrm{d}\vec{\mathbf{s}} = \mathrm{d}r\mathrm{d}z\hat{\boldsymbol{\phi}}$. Consequently,

$$\underline{I}_{eddy} = -\mathrm{j}\sigma\omega \int_{S'} \underline{A}_{\phi}\mathrm{d}r\mathrm{d}z. \tag{A.11}$$

It is also assumed that the dimensions of the conductor are at most of the same order of magnitude as δ, whereby only small variations of the magnetic vector potential along the surface of the conductor are to be expected. Thus, by factoring $\underline{A}_{\phi}$ out from the integral, the following equation can be obtained

$$\underline{I}_{eddy} = -\mathrm{j}\sigma\omega\underline{A}_{\phi} \int_{S'} \mathrm{d}r\mathrm{d}z. \tag{A.12}$$

It should be noted that the magnetic vector potential actually presents variations along the window of the transformer core, and also from one conductor to the adjacent one. However, simulations confirm that the variations of the magnetic vector potential within a conductor are very small compared to global variations when the conductors are of the same order of magnitude or smaller compared to δ.

On the other hand, the assumption that conductors have dimensions of the same order magnitude as δ is reasonable since the manufacturers use this criterion to keep eddy current losses under control. However,

care must be taken in using the methodology proposed in this work for conductors such as rods, bars or plates whose dimensions are in general much larger than δ.

Recalling that S' defines the cross-sectional area of the conductor, the surface integral is the conductor cross-section s_c, so that

$$\underline{I}_{eddy} = -\mathrm{j}\sigma\omega s_c \underline{A}_{\phi}. \tag{A.13}$$

It is emphasized that in this work the magnetic vector potential has not been merely used as a mathematical tool to reduce the dimensionality of the problem. In fact it has been given to the magnetic vector potential a true physical meaning. As it can be seen in Eq. (A.13), the magnetic vector potential has a direct relation with eddy currents in conductors. The physical effects of magnetic vector potential are experimentally evidenced in [13].

It can be shown from Eq. (A.8) that for a conductor which mean radius is r, the source current density $\underline{J}_{src}$ is related to the voltage drop $\underline{V}_{dp}$ as follows [12]

$$\underline{J}_{src} = -\frac{\sigma \underline{V}_{dp}}{2\pi r}. \tag{A.14}$$

By solving for the voltage drop in the conductor, the following expression can be obtained

$$\underline{V}_{dp} = -\frac{2\pi r}{\sigma}\underline{J}_{src}. \tag{A.15}$$

As in the case of the eddy current density, it is assumed that the source current density variation on the surface of the conductor is considerably small, which leads to the following equation

$$\underline{J}_{src} = \frac{\underline{I}_{src}}{s_c}. \tag{A.16}$$

Solving for $\underline{I}_{src}$ in (A.6) results in,

$$\underline{I}_{src} = \underline{I}_{\phi} - \underline{I}_{eddy}. \tag{A.17}$$

Substituting (A.17) into (A.16) yields,

$$\underline{J}_{src} = \frac{\underline{I}_{\phi} - \underline{I}_{eddy}}{s_c}. \tag{A.18}$$

Substituting (A.13) into (A.18) gives,

$$\underline{J}_{src} = \frac{\underline{I}_{\phi} + \mathrm{j}\sigma\omega s_c \underline{A}_{\phi}}{s_c}. \tag{A.19}$$

Substituting (A.19) into (A.15) gives the following expression for the voltage drop,

$$\underline{V}_{dp} = -\frac{2\pi r}{\sigma s_c}\left(\underline{I}_{\phi} + \mathrm{j}\sigma\omega s_c \underline{A}_{\phi}\right). \tag{A.20}$$

Rearranging,

$$\underline{V}_{dp} = -\underline{I}_{\phi} \cdot \frac{2\pi r}{\sigma s_c} - \mathrm{j}2\pi r\omega \underline{A}_{\phi}. \tag{A.21}$$

The mean length of the conductor can be defined as $l_m = 2\pi r$ from Eq. (A.21), and hence the DC resistance of the conductor is

$$R_{DC} = \frac{l_m}{\sigma s_c}. \tag{A.22}$$

Substituting the resistance and the mean length in Eq. (A.21) gives

$$\underline{V}_{dp} = -\underline{I}_{\phi} R_{DC} - \mathrm{j}\omega l_m \underline{A}_{\phi}. \tag{A.23}$$

References

[1] G. Diaz and E. Mombello, Semianalytic integral method for fast solution of current distribution in foil winding transformers, *IEEE Transactions on Magnetics* **51**(9) (September 2015), 1–9.

[2] L.D.S. Coelho, V.C. Mariani, F.A. Guerra, M.V.F. da Luz and J.V. Leite, Multiobjective optimization of transformer design using a chaotic evolutionary approach, *IEEE Transactions on Magnetics* **50**(2) (February 2014), 669–672.

[3] S.V. Kulkarni and S. Khaparde, *Transformer Engineering: Design and Practice*, CRC Press, 2004.

[4] D.A. Koppikar, S.V. Kulkarni, G. Ghosh, S.M. Ainapure and J.S. Bhavsar, Circulating-current loss in transformer windings, *IEE Proceedings - Science, Measurement and Technology* **145**(4) (July 1998), 136–140.

[5] B. Xia, G.G. Jeong and C.S. Koh, Co-kriging assisted pso algorithm and its application to optimal transposition design of power transformer windings for the reduction of circulating current loss, *IEEE Transactions on Magnetics* **52**(3) (March 2016), 1–4.

[6] X. Dexin, Y. Xiuke, Y. Yingying, B. Baodong and N. Takahashi, Circulating current computation and transposition design for large current winding of transformer with multi-section strategy and hybrid optimal method, *IEEE Transactions on Magnetics* **36**(4) (July 2000), 1014–1017.

[7] J.R. da Silva and J.P.A. Bastos, Analysis of power transformer geometry simplifications on electromagnetic and thermodynamic simulations, *IEEE Transactions on Magnetics* **51**(3) (March 2015), 1–4.

[8] G. Diaz and E. Mombello, New compact and singularity free formulations for the magnetic field produced by a finite cylinder considering linearly varying current density, *International Journal of Applied Electromagnetics and Mechanics* **50**(2) (2016), 483–501.

[9] G. Diaz and E. Mombello, Magnetic field due to a finite current carrying disk considering a variable current density along its radial dimension, *International Journal of Applied Electromagnetics and Mechanics* **42**(1) (2013), 119–136.

[10] P. Solin, I. Dolezel, P. Karban and B. Ulrych, *Integral Methods in Low-Frequency Electromagnetics*, John Wiley & Sons, 2009.

[11] H.E. Knoepfel, *Magnetic Fields: A Comprehensive Theoretical Treatise for Practical Use*, John Wiley & Sons, 2008.

[12] A. Konrad, Integrodifferential finite element formulation of two-dimensional steady-state skin effect problems, *IEEE Transactions on Magnetics* **18**(1) (January 1982), 284–292.

[13] M. Daibo, S. Oshima, Y. Sasaki and K. Sugiyama, Vector potential coil and transformer, *IEEE Transactions on Magnetics* **51**(11) (November 2015), 1–4.